Mem. S.A.It. Vol. 93, 224

Memorie della

Increase of the Technological Readiness Level for the realization of hard X-/soft gamma-ray Laue optics

E. Virgilli[1,2], L. Ferro[3], C. Ferrari[4], R. Lolli[3,4], S. Squerzanti[5], F. Frontera[3,1], P. Rosati[3,1,5], O. Limousin[3], N. Auricchio[1], E. Caroli[1], M. Moita[3], M. Pucci[7], J. B. Stephen[1], C. Gargano[6], S. Del Sordo[6], and C. Guidorzi[3,1,5]

[1] INAF – OAS, Via Gobetti 101, I-40129, Bologna, Italy, e-mail: enrico.virgilli@inaf.it
[2] INFN-Sezione di Bologna, Viale Berti Pichat 6/2, I-40127 Bologna, Italy
[3] Dipartimento di Fisica e Scienze della Terra - Università degli studi di Ferrara - via G. Saragat 1, I-44122, Ferrara, Italy
[4] IMEM/CNR Parco Area delle Scienze 37/A, I-43124 Parma, Italy
[5] INFN Sezione di Ferrara - via G. Saragat 1, I-44122 Ferrara, Italy
[6] INAF – IASF Palermo, Via Ugo La Malfa 153, I-90146 Palermo, Italy
[7] CNR - Istituto Nazionale di Ottica - Largo Fermi 6, I-50125 Firenze, Italy

Received: 17 January 2022; Accepted: 17 June 2022

Abstract. A number of key problems in astrophysics are unanswered due to the limited sensitivity of the present instrumentation in the X and gamma energy band. Laue lenses based on diffraction in crystals offer an effective solution to this problem. The potential of Laue lenses is linked to the massive production of curved crystals and to the quality of the alignment process which must be performed with an accuracy better than 30 arcsec. Within the project, an advancement in the TRL (Technology Readiness Level) has been pursued in recent years. Such a technological improvement could be exploited first in a balloon experiment and, ultimately in a space mission telescope with a few tens of meters focal length, capable of focusing incoming high energy photons with a broad energy pass-band.

Key words. – Laue lenses – Soft gamma-rays – X-ray diffraction – Bragg law – Hard X-ray astrophysics – Hard X-ray optics

1. Introduction

The soft gamma-ray band from tens of keV up to several hundreds of keV is of crucial importance for the understanding of several astrophysical processes. It contains most of the nuclear lines emitted in the decays of radioactive nuclei associated with synthesis of the chemical elements, as well as the positron annihilation radiation that is the first direct probe of antimatter in the Universe. The hard X-/gamma-ray regime is also the band in which many astrophysical systems emit most of their en-

ergy mainly through mass accretion onto compact objects. Despite its fundamental role in addressing the above subjects and many other, hard X-/soft gamma-ray astrophysics suffers from low sensitivity and poor image reconstruction capability, when compared to what is technologically feasible at lower or at higher energies. Up to ∼10 keV grazing incidence optics have been pushed to reach sub-arcsecond resolution. From ten up to 70-80 keV, multilayers allowed the generation of images with sub-arcmin resolution. In the MeV regime the pair production process allows the direction of the incoming photon to be deduced. In the hard X-/soft gamma-ray range (0.1 - 1 MeV) grazing incidence optics is impractical (the graze angles are extremely small) and the dominant Compton interaction process provides only limited directional information. At these energies where grazing incidence optics are not effective, only one technology, based on diffraction from crystals, is available for focusing gamma-rays. Laue lenses use diffraction from an array of properly arranged and oriented crystals, thus providing a high level of concentration of the flux from on-axis sources. Nevertheless, this technique is, at the state of the art, still in a development phase due mainly to the extraordinary accuracy required for the realization of the optics which consists of several single optical elements to be optimized and assembled.

Recently, within the ESA Voyage 2050 call, two mission concepts including Laue lenses have been proposed, demonstrating the interest in this technology by the scientific community. In Phemto (Laurent et al. 2021), led by France, a Laue lens with 100 m focal length (FL) is proposed in combination with an Athena-like soft X-ray optics based on Silicon Pore Optics (SPO) (Bavdaz et al. 2012). The proposed focal length will be obtained most probably in a formation-flying configuration. The second mission named ASTENA (Frontera et al. 2021; Guidorzi et al. 2021) consists of a Narrow Field Telescope (NFT) based on a 20 m FL Laue lens with 50 - 700 keV energy passband and of an array of Wide Field Monitors with Imaging and Spectroscopic capabilities (WFM-IS) based on two-scale coded mask apertures. Simulations and laboratory experiments have demonstrated the advantages of using this technology. In order to increase its maturity, within this approved project (hereafter called TRILL - Technological Readiness Improvement of Laue Lenses) we have investigated how to increase the readiness of the Laue lenses with respect to the current state-of-the-art.

2. Goals of the TRILL project

Hard X-/soft gamma-ray astronomy requires an improvement of the current technology. Firstly, sub-arcminute angular resolution is desirable, but the Point Spread Function (PSF) achievable with the classical coded mask technique is of the order of few arcminutes. Such a leap in angular resolution could be achieved through the use of Laue lenses. However this goal is not trivial if flat crystals are used, as the angular resolution depends on both the crystal size and the Laue lens FL. For instance, flat crystals with cross section 1×1 cm^2 and a 20 m FL corresponds to an angular resolving power (α_{rp}) of the order of 1.7 arcminutes which is comparable with that achievable with coded mask techniques (e.g. for INTEGRAL/JEM-X, $\alpha_{rp} \sim 3$ arcmin, for WFC/BeppoSAX, $\alpha_{rp} \sim 5$ arcmin, for CZTI/AstroSAT, $\alpha_{rp} \sim 8$ arcmin). The smaller the crystals size or the longer the FL, the better the achievable α_{rp}. However, a small crystal size implies a large number of them, with increasing difficulties in the overall alignment. Contextually, FL larger than 15-20 m appears less feasible for the demanding stability required for the expandable structure or for the technological complications induced by the adoption of a formation-flying configuration.

Bent crystals can overcome the above limitation given that their diffracted signal is smaller than the crystal cross section itself. Thanks to the bent crystals a PSF comparable to NuSTAR (60" HPD, 18" FWHM) or even better (the goal of the TRILL project is 30 arcsec) with a comparable focal length can be achieved.

Three main goals drive the TRILL project: the **first** objective is to identify the best ma-

terials and geometrical configurations in order to maximize the throughput of the Laue lens. In particular, we have defined a repeatable, affordable and fast method to obtain self-sustained bent crystals. To this end, we have considered perfect bent crystals made of Germanium and Silicon whose diffraction planes are the (110). Differently from previously adopted mosaic Gallium Arsenide (GaAs) crystals, Ge and Si are perfect crystals with a few arcseconds angular spread (of the order of the Darwin width). We have also planned to use Ge and Si crystal with different diffraction planes (111) to exploit the so-called secondary curvature of the diffraction planes that considerably increases their diffraction efficiency above the limit of the 50% of mosaic and perfect crystals (Bellucci et al. 2016; Camattari et al. 2011). Their cylindrical curvature radius of 40 m, which is twice the focal length of the Laue lens, ensures a continuous energy pass-band. The **second** objective of TRILL is to find a reproducible and reliable method for the assembly of a large number of tiles in a reasonable short time, with affordable cost and with long term stability. These features all together are not simple to be achieved. Nevertheless new materials and technologies can be useful for these goals. Finally, the **third** objective is to achieve an overall system maturity, meaning that besides the Laue optics development a suitable focal plane detector must be adopted. We demonstrate that the most appropriate detector is a solid state device with both spectroscopic and imaging capabilities that can also provide information about the polarization degree of the focused radiation.

In the next Sections we will go through these three different aspects by describing the advancement achieved and the encountered limitations.

3. Production of suitable crystals

Germanium and silicon crystal tiles with cross section 30×10 mm^2 have been used in the TRILL project. Planar wafers of Silicon (001) with diameter of 4" are used to cut $\sim$ 15 crystal tiles (Fig. 1). The diffraction planes are the (110) parallel to the 10×2 mm^2 edge with a cut uncertainty of the order of 0.2 degrees. Also the miscut angle between the external main surface and the perpendicular to the diffraction planes is of the order of a few tenths of a degree. The crystals are cleaned and worked with a surface lapping process on one of the two large surfaces. Such a process induces a surface strain that is responsible for a self-sustained cylindrical curvature of the crystals (Bonnini et al. 2015; Ferrari et al. 2020). The method for bending the sample has been developed thanks to previous financed projects (e.g. the LAUE project (Virgilli et al. 2014)). Nevertheless, the accuracy of bending such crystals with a curvature of the order of 40 m was poorly reproducible within an accuracy of the order of 10%. Thanks to the new lapping machine Accura 102 (Metkon), the bending method has been improved up to an accuracy of the order of 2% . Furthermore the process has been made faster thanks to the custom designed floating head that allows three tiles to be worked simultaneously (see Fig. 2). It has been experimentally proven that after the process, the 3 crystals display the same curvature radius within the uncertainty.

The available lapping machine allows various parameters to be set and finely tuned in order to optimize the machining process for achieving the correct curvature radius (time of lapping, 4 types of roughness of the lapping surface 18, 54, 75, 125 μm, speed of the process and the direction of rotation, force applied to the lapping head). A reliable set of parameters and consequently a reproducible bending technique has been defined for crystals with thicknesses of the order of 1.8-2 mm.

Several tens of crystals have been worked in order to achieve the nominal curvature radius of 40 m. The mean curvature radius of the normal distribution is 39.3 m with *sigma* = 1.0 m which satisfy the requirement for the crystal production. However, further tests are being performed in order to define the set of parameters through which thicker crystals can be correctly bent at the same curvature radius. This request is driven by the fact that, while at energies below 150 keV the thickness maximizing the diffraction efficiency approaches

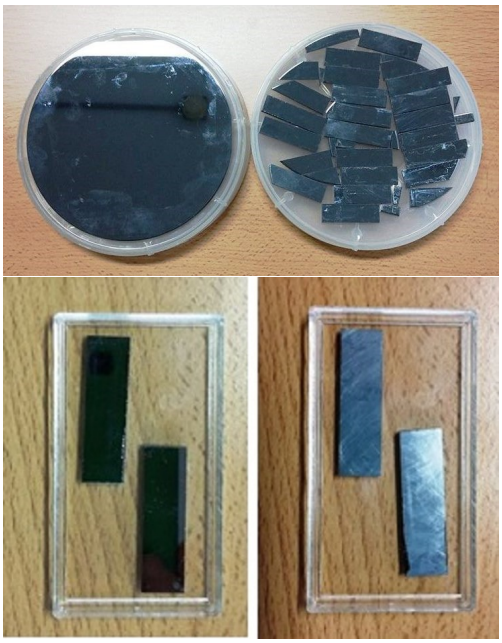

Fig. 1. Top: wafer of Germanium (001) cut in tiles with cross section 10×30 mm^2, 2 mm thick. The diffraction planes, oriented as the 10×2 lateral surfaces, are the (110). From a single wafer 15 - 16 tiles can be obtained. Bottom: crystal tiles before and after the process of mechanical lapping.

Fig. 2. Top view of the rotational head of the lapping machine through which three crystals can be machined at once. The floating head allows to impress the same strength over the three crystals therefore the same curvature radius is achieved for the three sample with few percent of uncertainty.

2 mm, at higher energies the optimized thickness is larger (up to 5 mm).

After the crystals preparation their curvature has been estimated both in Bragg (reflection, measurement campaign made at CNR/IMEM - Parma) and in Laue (transmission, made at LARIX - Ferrara) configuration. The method for the curvature radius estimation consists of impinging with an X-ray pencil beam on the crystal surface along its cylindrical profile and to acquire the diffracted signal by shifting the beam at regular spatial intervals on the crystal. High resolution X-ray diffraction measurements have been performed in Bragg geometry by means of a X'Pert PRO Philips diffractometer equipped with a four 220 Ge monochromator (CuKα1 radiation, λ = 0.15405 nm). The rocking curve peak shift, as a function of the position at which the beam impinges on the sample, provides an estimate of the sample curvature radius. In Fig. 3 are shown two examples of curvature radius estimation. A similar approach has been adopted at the LARIX facility by using a polychromatic beam and by estimating the curvature of the sample by measuring the energy variation of the diffracted signal in transmission configuration. The two methods gave consistent results within 2% uncertainty. The uncertainty can be ascribed to the different adopted configuration that involves the surface of the crystal in the reflection case and its full depth in the transmission case.

By using a planar Si (001) wafer the spurious curvature originating from the uncertainties of the rotation and translation stages used in the experiment has been estimated. This residual curvature radius has been quantified in ~800 m which is a negligible curvature for our purposes. Nonetheless, this quantity can be taken into account and subtracted from the measurement of the unknown radius in order to estimate the real curvature radius of the sample.

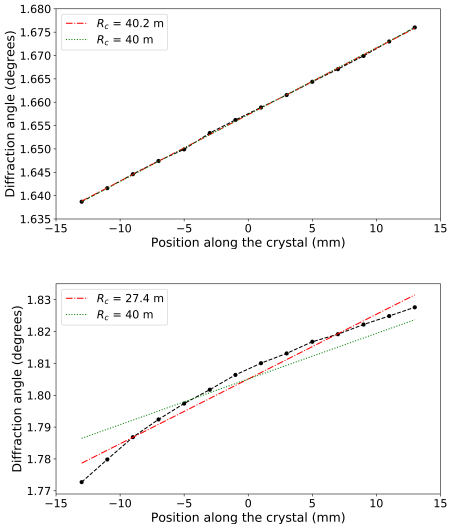

Fig. 3. Example of curvature radius estimation for two bent Germanium crystals. In the X-axis is reported the position of the X-ray pencil beam along the crystal while in the y-axis the corresponding angles required to diffract the Cu Kα_1 are reported. Black points represents the acquired data, black line connecting the data defines the local curvature radius as the angular coefficient of the line is the reciprocal of the curvature radius. Red line is the best fit line from which the average curvature radius can be determined. Green line describes the best fit corresponding to 40 m curvature radius (goal of the project). Top: crystal with highly accurate curvature radius (the three different lines are superposed and indistinguishable). Bottom: crystal with strong irregularities in the curvature radius.

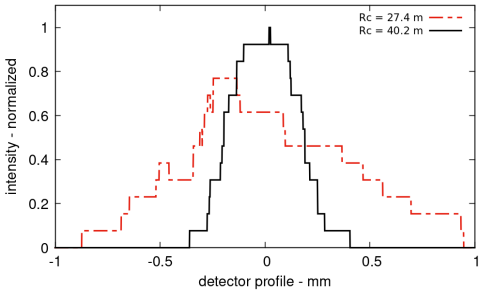

Fig. 4. Estimation of the diffracted profile on the detector plane positioned at 20 m from the crystals. Two crystals with different curvature radius are shown (the same reported in Fig. 3). On the x-axis are the X-ray positions on the detector while the y-axis represents the normalized intensities of the collected signal. For a curvature radius of 40.2 mm the signal is fully collected in 0.37 mm (FWHM) on the detector plane. For the crystals with inhomogeneous curvature radius the profile on the detector is almost 2 mm wide (0.85 mm FWHM).

3.1. Crystals selection criteria

The imaging response from a bent crystal can differ from its nominal shape due to two main factors that are hereafter discussed. Both are related to the inhomogeneity of their curvature. We do not discuss in this paper how to correct and minimize such effects for each crystal. We limit the discussion to the definition of acceptance or rejection criteria. To this end, Python codes have been developed in order to discretize and quantify the shortcomings. The first effect is related to the uniformity of the crystal curvature. With reference to Fig. 3 we have evaluated:

i) the curvature radius of the segment $k - th$ (i.e. the angular coefficient m_k of the segment that connect the points k and $(k + 1)$. Such segment corresponds to a fraction of the crystal that exhibit a local curvature radius different from the average curvature radius and, more importantly, from the nominal curvature radius $m_n = 40$ m. The deviation of m_k from m_n corresponds to a broadens of the diffracted signal;
ii) the orientation of the segment $k - th$ with respect to the focal point. The mis-orientation of the segment can be quantified by evaluating the intercept q_k (y value at x = 0). This effect does not induce a broadening of the signal but the local diffraction is shifted from the nominal focal point.

The two contributions combine for every single segment of the crystal and the overall effect is to enlarge the PSF. In Fig. 4 is shown the estimation of the 1-dimension profile of the photon distribution on the detector for the two crystals whose curvature radius estimation is shown in Fig. 3. As can be observed for the ∼40.3 m curvature radius the width of the signal is less than 0.5 mm (FWHM). This quantity rapidly increases as the local parameters m_k and q_k deviate from their nominal values.

The second type of inhomogeneity results in a twisted diffracted image which contributes to the overall worsening of the nominal Laue lens PSF. This possibility is exemplified with the sketch of Fig. 5. In Fig 6 (a, b) are shown two examples of measured diffracted signals. Such a shape can be due to a deformation of the perfect cylindrical shape of the crystals. This can be due to a torsion caused by the growing process or, more likely, due to the mechanical process used to bend the crystal.

In order to discretize the described effect and to identify a quantity that would drive the rejection or the acceptance of a crystal we have divided the crystal in 36 layers. Each slice provides a fraction of the cumulative diffraction signal. The different position is due to a different orientation of the slice with respect to the nominal configuration. We fitted the diffraction profile with a generalized Gaussian function:

$$f(E) = I_0 \, e^{-\frac{(E-E_0)^p}{2\,\alpha^p}} \qquad (1)$$

The chosen number of layers is a trade off between a sufficient number of collected photons for each layer and the width of the layer itself. In Fig. 6 (c, d) the discretization of the previously mentioned diffracted signals are shown. The width of the rectangles represents the FWHM of the signal that depends on the local curvature radius (the more out of focus is the crystal layer, the larger is the FWHM). An excess of deformation with respect to the ideal diffracted shape will degrade the overall PSF, therefore a rejection criterion must be established. We set the limit of the distribution to 10 arcsec (see Fig 6-e).

No correlation has been found between the amplitude of the deformation and the curvature radius of the crystals. The crystal warp can be already present before the bending process, or more likely, is induced by the surface lapping. Further study must be performed in order to understand its origin and to minimize its effects on the PSF.

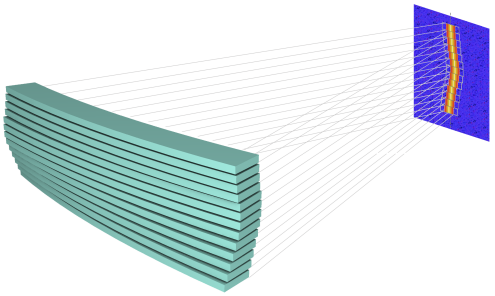

Fig. 5. Illustration of the distortion diffraction from a bent crystal. A physical twist of the crystal, due to defects in the growing process or to the bending process, can explain this effect. In order to evaluate the amount of deformation, the crystal is though ideally subdivided in thin layers. Each layer focus the radiation at different position of the focal plane detector with respect to the nominal position.

4. Crystals assembly method

One of the main goals of TRILL is to position tens of crystals per module with an accuracy of the order of 10 arcseconds. The crystals are set and oriented under the control of an X-ray source. As heritage from previous projects, we make use of an adhesive for bonding the crystal at their correct orientation over a common substrate. Both the crystals and the substrate are kept vertical therefore the adhesive must have sufficient viscosity in order not to fall off after being deposited, before polymerization. Much effort for minimizing the uncertainty in the assembly of the crystals has been expended in order to achieve an accuracy better than 30 arcsec during the mounting process. The long-term stability (months-years) must be evaluated to demonstrate its tchnological readiness for its use on a space experiment. A 5 mm thick bent substrate made of quartz has been used for the assembly. The choice has been driven by different factors:

i) the adopted bonding method exploit an UV curable adhesive with very low shrinkage. Its curing time of a few seconds allow a very fast assembly. The quartz has been chosen as it is sufficiently transparent to the UV light;

ii) the 5 mm thick quartz has a transmission of ~84% for 150 keV energy photons. Such a thickness is a trade off between absorption and sufficient strength and stability of the substrate;

iii) the quartz has a thermal expansion coefficient of 5.5×10^{-7} K^{-1} providing a high ther-

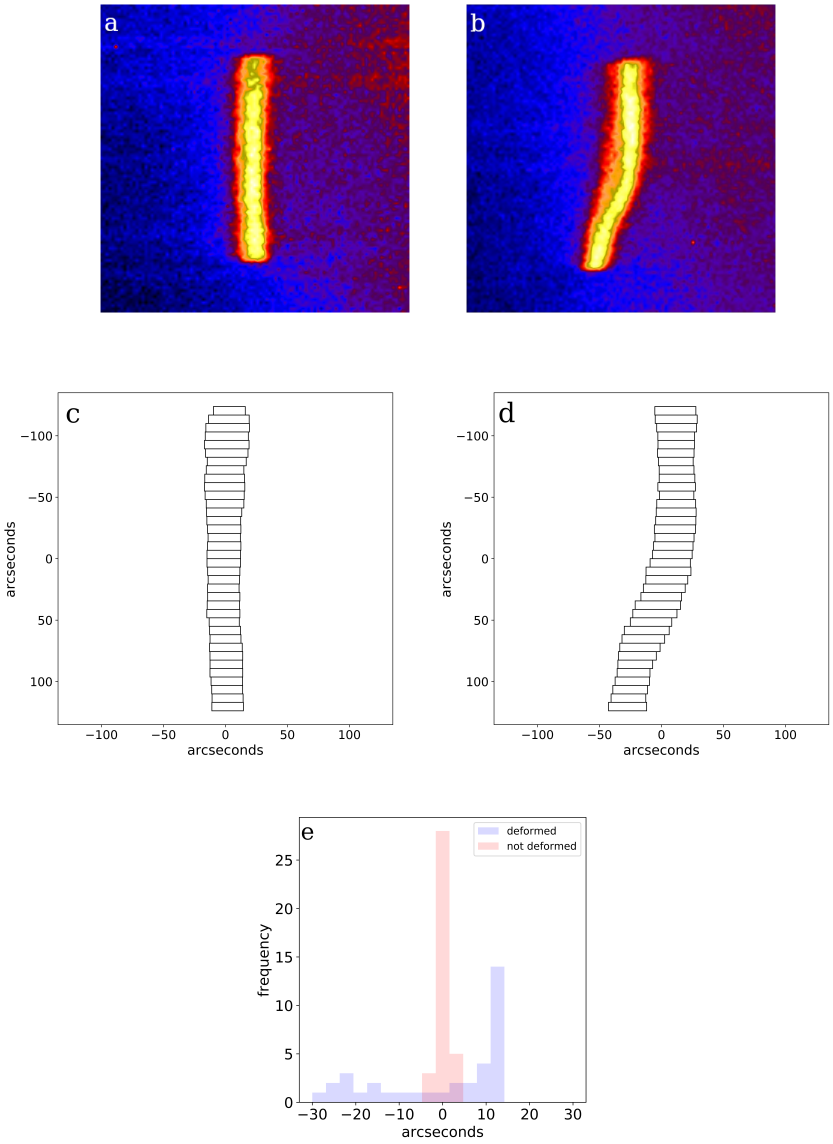

Fig. 6. *Top*: Two measured diffracted images collected at the focal plane if their 30×10 mm^2 cross section is fully illuminated. The centroid of the diffracted energy is 150 keV. *Center*: the same two diffracted images discretized in 36 layers. The width of the rectangles are the FWHM of the diffracted signals (different for each slice). *Bottom*: histogram describing the spatial distribution of the radiation on the focal plane detector for the crystal whose response is close to the nominal response (red histogram) and for the crystal that suffers from deformation (blue histogram).

mal stability during the bonding process and for long terms monitoring.
Other possible materials under evaluation are Zerodur glass ceramic for its extremely low expansion coefficient and low density (CTE $\sim 0.2 \times 10^{-7}$ K^{-1}, $\rho \sim 2.21$ g/cm^3) (Shiou & Asmare

2015; Banyal et al. 2013; Jedamzik et al. 2013) and ULE - Ultra Low Expansion Titanium Silicate glass (CTE = $0 \pm 30 \times 10^{-9}$ K^{-1} in the range 5 - 35 °C, 95% confidence level and $\rho \sim 2.21$ g/cm^3) for its low density and stability. An interesting solution could be the use of 3-d printable polymers like ULTEM™ 9085 which is a space qualified high-performance thermoplastic already used for space experiments like the Mini-EUSO telescope (Bacholle et al. 2021) installed on the ISS. The back and front main surfaces of the quartz substrate have been finely worked at CNR/INO Arcetri (Florence, Italy) in order to have a flat surface on one side and a bent surface with 40 m curvature radius on the other side. A gauge for deflection measurement with accuracy of 1 μm has been used to measure the curvature radius. This accuracy corresponds to an estimate of the curvature radius of the substrate better than 0.3 m for 40 m curvature radius goal and, with a substrate length of $\sim$ 25 cm. This allows the cylindrically bent crystal (40 m curvature radius) to be set parallel to the substrate surface by minimizing the layer of adhesive which is of the order of 50 - 100 μm. The substrate has been worked with a satin finishing (surface roughness $\sim$1 μm). Further development under consideration is to optically finish the surface so as to minimize the potential non-uniformity of the adhesive between crystal and substrate. The substrate is held with an INVAR steel frame with CTE $\sim 1.2 \times 10^{-6}$ K^{-1} which is almost 10 times smaller than that of ordinary stainless steel.

Two modules of Laue lenses have been assembled (see Fig. 7). The first was realized with 16 crystals made with Gallium Arsenide (GaAs), already available. In order to avoid accidentally touching one crystal while mounting the next, the separation between the crystals has been left to the order of 1.5 mm. With this separation the filling factor of the module is of the order of 87%. A second module was realized by using the first 11 crystals made of Ge(220) from the first batch provided by IMEM Parma. Also in this case the separation between the crystals was on average 1.5 mm due to the alignment of the crystals in both directions (Bragg angle θ_B and azimuth angle ϕ).

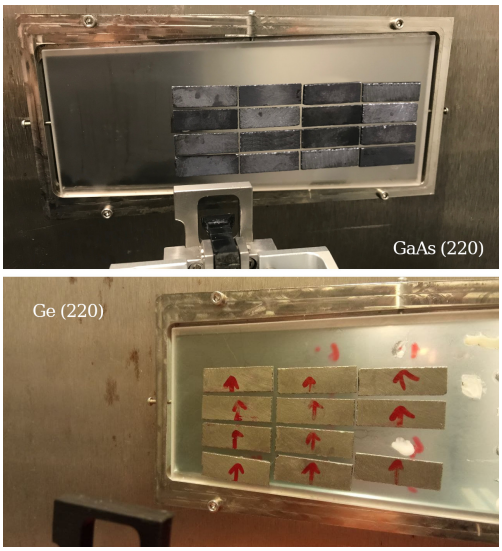

Fig. 7. Two modules made with 16 GaAs crystals and 11 Ge crystals (top and bottom, respectively) realized with the use of a quartz substrate inserted in a INVAR frame. The crystals are bonded over the substrate with a UV curable adhesive. The polymerization time of the order of few seconds.

The main differences between the two modules are the parameters of the UV lamp used for the polimerizaton of the adhesive. In both cases the achieved accuracy in mounting the crystals is several tens of arcseconds with respect to the goal of 10 arcsec (see Fig. 8). More trials are being made in order to further reduce this uncertainty.

5. Alternative assembly and alignment methods

Orienting and bonding the crystals by using glues have some evident difficulties. Experimental tests have confirmed that the use of adhesives is critical for an accurate positioning of the crystals. Typically, the uncertainty increases with the thickness of the adhesive layer. Instead, once cured, the adhesive does provide a sufficient long term stability, that depends on the type of glue that is used. The polymerization of the glue generates a stress that tilts the crystals out of the nominal position with consequent variation of the direction of

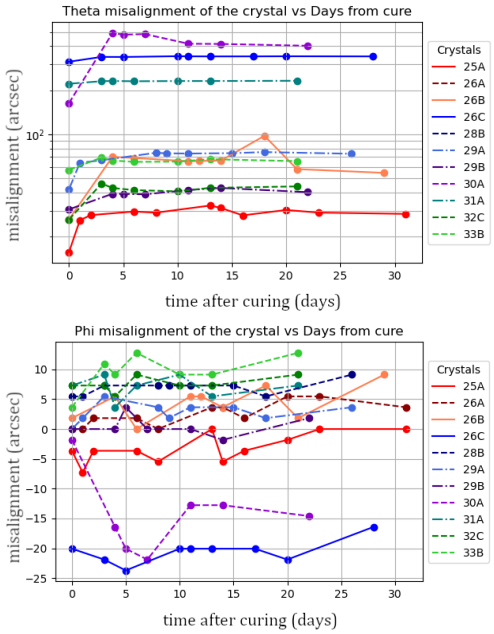

Fig. 8. Top: Misalignment on the Bragg's angle position (θ-misalignment) vs days from cure for the 11 crystals of the Ge module. Bottom: Misalignment on the azimuth position on the spherical lens surface (ϕ-misalignment) vs days from cure for the 11 crystals of the Ge module.

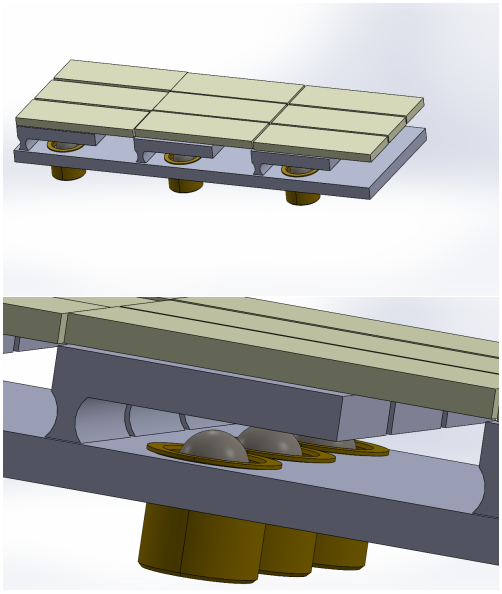

Fig. 9. Top: 3-d model of a prototype of deformable substrate (grey part) with nine crystals (yellow parts) fixed on the lamellae. Bottom: detail of the structure composed by a bottom layer with a hole in which a micrometric screw is inserted. Each crystal is fixed on the top of a lamella. The orientation of each crystal is obtained by orienting the lamella through the micrometric screw. The lateral flexure hinge reacts to the induced force and keeps the crystal at the correct orientation.

the diffracted signal from its nominal position. The result is that the focusing power is reduced due to the broadening of the cumulative PSF with respect to the nominal alignment. Such uncertainty cannot be fully canceled as the direction of the unwanted torque due to the glue polymerization phase is mostly unpredictable and mainly depends on sub-micrometric irregularities of the crystal and/or of the substrate and/or of the adhesive layer. These considerations lead to the research of alternatives bonding and alignment methods.

We investigated the possibility of orienting the crystals by exploiting a 3-d printable, low X-ray absorption and very light substrate, through microthread screws and by means of zero-clearance flexure hinges. A 3-d model through which it is possible to position a number of tiles is shown in Fig. 9. As visible in Figure the alignment system consists of a monolithic object made by a layer in which a hole per slot is drilled. Each crystal is fixed through an epoxy adhesive on the top of a lamella which is an elastic structure fixed over the substrate. In this case the adhesive, which has been demonstrated to have a good long term stability, is being used only for bonding, while, previously its function was also to keep correctly oriented the tile. At its rest position the lamella is parallel to the substrate. A 508 thread per inch (TPI) high precision commercial screw with 50 μm pitch is placed on the bottom of each crystal location. The function of the screw is to pushes the lamella and orient the crystal at the correct diffraction angle. The flexure hinges are dimensioned in order to strongly and elastically react to a deformation of 2 degrees which is twice the maximum Bragg angle required for the diffracted energy of this prototype. Higher angular dis-

placements can be achieved with a proper design of the ratio between the lamella and the hinge thicknesses. The material for the substrate can be plastic, aluminum, carbon fiber. An interesting solution could be the ULTEM™ 9085 space qualified high-performance thermoplastic. For the first test, a model consisting of 6 slots is being realized with a 3-d printed Acrilonitrile butadiene stirene (ABS). The results will be made available by the end of the TRILL project. It is worth noting that the correct orientation of a crystal would require at least two angular tilts, one for the Bragg angle and one for the tilt around the axis of the impinging X-ray beam. Nevertheless, the Bragg angle orientation is the most critical angle therefore a single tilt correctly aligns a crystal with good approximation. One aspect of this proposed method that must be carefully evaluated is the transparency of the overall system to the radiation that must pass through the whole alignment structure. The 3-d printed substrate (3 mm substrate + 3 mm lamella) allows 91% transparency at 150 keV. On the other hand, the alignment screws and the corresponding sockets have an overall diameter of 8 mm per crystal. With the very conservative assumption that the structure is fully opaque this corresponds to 15% of lost area. However, commercial-off-the-shelf screws can be replaced with custom miniaturized alignment screws allowing to further reduce the covering factor well below 10%.

One critical point that must be addressed is that the few mm thick crystals, particularly suitable for diffracting < 100 keV photons, are easily deformable during the adhesive polymerization phase. However, the function of the adhesive is to firmly hold the two parts therefore a deformation due to the bonding phase has been frequently observed, especially for the lowest adhesive thicknesses (< 50 μm, i.e. when the crystal is very close to the rigid substrate). An attempt to strengthen the crystals has been done by encapsulating one tile within two layers of epoxy adhesive (Fig. 10) It has been observed that such films protect the crystal from the unwanted effects of deformation due to the adhesive. Thicker crystals, suitable for higher energies, will not suffer from such defects as they will be more rigid and non-deformable under the effect of the bonding. On the other hand, thicker crystals will be harder to bend therefore other methods of self-sustained curvature must be investigated.

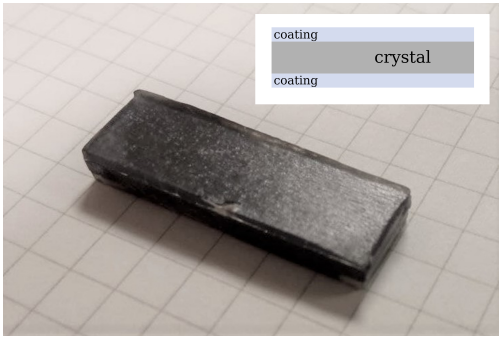

Fig. 10. Crystal coated with epoxy resin. A layer of ~1 mm of epoxy was cast inside a silicon mold, then the crystal was placed on top of it and, finally, another layer of ~1 mm was cast on top of the crystal. After the cure, the surfaces of the crystal were polished. The final size of the coated crystal is 30×10×4.5 mm^3.

6. Focal plane detector units

For the assembly of the crystals and for the final tests on the modules two detectors have been used. An Ortec pop-top High Purity Germanium detector (HPGe) with 550 eV energy resolution at 122 keV is used for spectroscopic information. A Perkin Elmer flat panel is used for imaging purposes (200 μm spatial resolution). The two instruments works independently and are placed on a 3-stages motorized rail in order to set one of them at the focal point of the module. From a technical point of view, such a configuration prevents the simultaneous acquisition of both spectral and positional information during the lens modules assembly. From the scientific side, a single detector capable of doing spectroscopy and imaging would have a significant impact on the instrument scientific performances. We have carried out a market research to find the solution fitting with the requirements. In particular, we have evaluated the ComptonPOLCA, developed at LIP-

Table 1. Main properties of the Caliste and of the ComptonPOLCA detectors that are under test for being used as focal plane detector.

	Caliste-O	Caliste-HD	Compton POLCA
Material	CdTe	Cd(Zn)Te	CdTe
Sensitivite area (cm^2)	1.4×1.4	1×1	1.6×1.6
Thickness (mm)	2	1	2
Pitch (mm^2)	0.8×0.8	0.625×0.625	2.0×2.0
Pixel array	16×16	16×16	16×16
Passband	2 keV - 1.2 MeV	2 keV - 1 MeV	40 keV - 1 MeV
Energy resolution	1.5% @ 60 keV	1.1% @ 60 keV	8.3% @ 278 keV

Fig. 11. The Caliste-HD (top) and the ComptonPOLCA (bottom) detectors that are being evaluated as focal plane detectors for the Laue lens modules.

Coimbra (Caroli et al. 2018) and two spectroscopic imagers named Caliste-O and Caliste-HD (Meuris et al. 2011; Maier et al. 2018) developed by CEA. The ComptonPOLCA and the Caliste-HD are shown in Fig. 11. The ComptonPOLCA is a prototype made with 2 layers Compton configuration based on two CdTe spectro-imagers operated in coincidence. The two CdTe detectors have one anode segmented in 8 × 8 pixels (2 mm pitch) on 2 mm thick crystals. The detection system configuration allows to assess and optimize the scattering polarimetric performance of a 3D spectro-imager by changing the distance between the two layers over the 100-600 keV energy range. The two Caliste devices consist of a pixel sensor, an electronic case containing the IDeF-X front-end ASICs and a pin array to connect the module to the electronic board. In particular, the pixel sensor is a Schottky Al/CdTe/Pt detector with a very low leakage current (< 10 pA). The Caliste detectors modules are fully compliant with operation in space (tolerant to radiation, thermal and mechanical constraints). The characteristics and performances of Caliste-O, Caliste-HD and ComptonPOLCA are summarized in Table 1.

7. Conclusions and future prospects

The TRILL project is characterized by a strong multidisciplinarity. It involves astrophysical knowledge, necessary for the definition of the science case and of the requirements of an in-

strument based on Laue lenses. It strongly involves technological aspects as new methods for the realization of suitable crystals and their alignment are being studied. It touches mechanical and material engineering knowledge that are necessary for a technology which is in a strong development phase. A dominant contribution is given by crystallography whose expertise allows, through simulation, both the identification of the material with the higher diffraction efficiency and the experimental development of the optical elements. A deep knowledge of the state of the art of the detection technology is also required for the optimization of the overall system. In the TRILL project we have tackled three aspects of the Laue Lens technology which are crucial for the goal of reaching a maturity required for a future use of Laue lenses in a balloon or in a space experiment. In this paper we have shown the main results of the project:
i) the advancement of a technology for the production of bent crystals with the proper self sustained curvature;
ii) further studies of a robust alignment method for assembling a large number of crystals with the required accuracy which must be kept stable for the entire duration of the experiment/mission;
iii) an evaluation of the performances of a suitable detector with spectroscopic imaging and polarimetric capabilities, to fully exploit the Laue lens potential. At present we are testing the spectroscopic and imaging performances of the Caliste-HD at INAF-OAS Bologna before its use as the focal plane detector for the realized Laue lens modules.

Acknowledgements. The financial support through ASI-INAF agreement n. 2017-14-H.0 is deeply acknowledged.

References

Bacholle, S., Barrillon, P., Battisti, M., et al. 2021, The Astrophysical Journal Supplement Series, 253, 36
Banyal, R. K., Ravindra, B., & Chatterjee, S. 2013, Optics Express, 21, 7065
Bavdaz, M., Wille, E., Wallace, K., et al. 2012, in Society of Photo-Optical Instrumentation Engineers (SPIE) Conference Series, Vol. 8443, Society of Photo-Optical Instrumentation Engineers (SPIE) Conference Series, 29
Bellucci, V., Camattari, R., Paternò, G., Guidi, V., & Mazzolari, A. 2016, Journal of Applied Crystallography, 49, 1810
Bonnini, E., Buffagni, E., Zappettini, A., Doyle, S., & Ferrari, C. 2015, Journal of Applied Crystallography, 48, 666
Camattari, R., Bellucci, V., Guidi, V., & Neri, I. 2011, in Optics for EUV, X-Ray, and Gamma-Ray Astronomy V, Vol. 8147
Caroli, E., Moita, M., da Silva, R., et al. 2018, Galaxies, 6, 69
Ferrari, C., Beretta, S., Rotunno, E., Korytár, D., & Zaprazny, Z. 2020, Journal of Applied Crystallography, 53, 629
Frontera, F., Virgilli, E., Guidorzi, C., et al. 2021, Experimental Astronomy, 51, 1175
Guidorzi, C., Frontera, F., Ghirlanda, G., et al. 2021, Experimental Astronomy, 51, 1203
Jedamzik, R., Kunisch, C., & Westerhoff, T. 2013, in UV/Optical/IR Space Telescopes and Instruments: Innovative Technologies and Concepts VI, ed. H. A. MacEwen & J. B. Breckinridge, Vol. 8860, International Society for Optics and Photonics (SPIE), 200 – 210
Laurent, P., Acero, F., Beckmann, V., et al. 2021, Experimental Astronomy, 51, 1143
Maier, D., Blondel, C., Delisle, C., et al. 2018, Nuclear Instruments and Methods in Physics Research Section A: Accelerators, Spectrometers, Detectors and Associated Equipment, 912, 338–342
Meuris, A., Limousin, O., Gevin, O., et al. 2011, in 2011 IEEE Nuclear Science Symposium Conference Record, 4485–4488
Shiou, F.-J. & Asmare, A. 2015, Precision Engineering, 42, 93
Virgilli, E., Frontera, F., Valsan, V., et al. 2014, arXiv e-prints, arXiv:1401.4948